Energy and Technology Review

Lawrence Livermore Laboratory January 1977

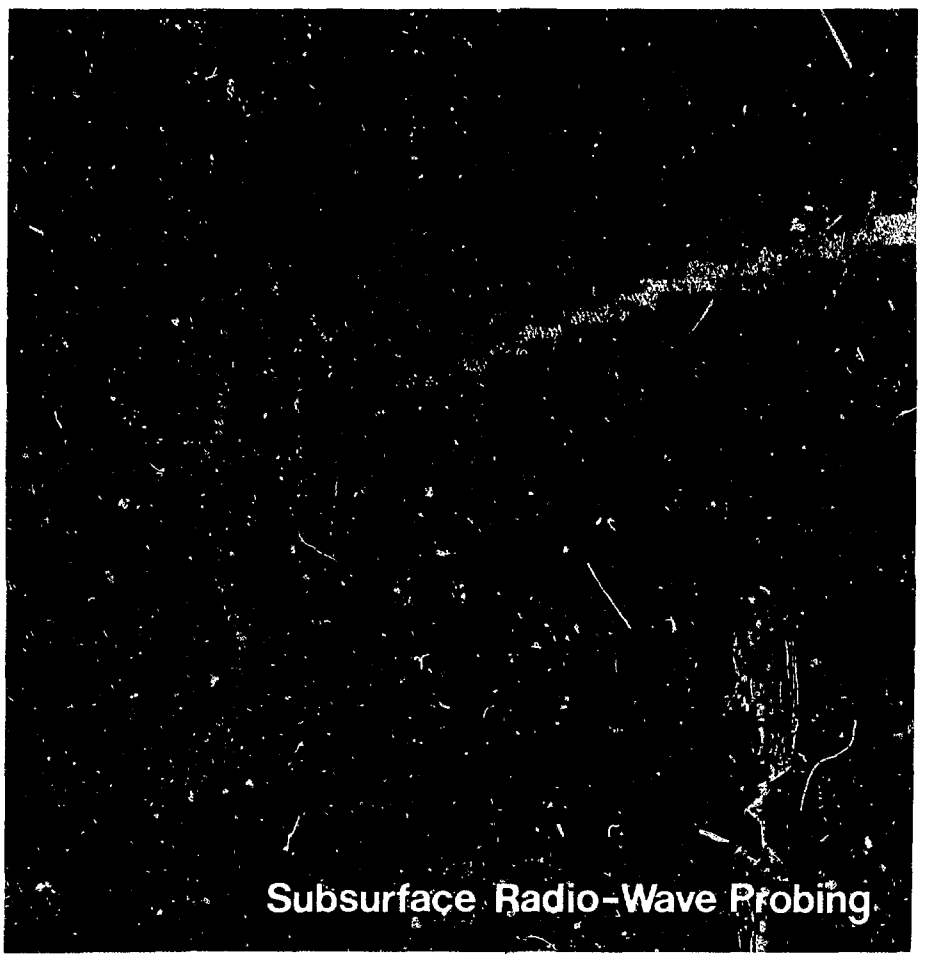

THE COVER

Diffraction pattern from a computer code used in our theoretical modeling studies of subsurface radio-wave probing. With this probing technique we can map an underground region and identify such anomalies as tunnels, sand lenses, and water pockets. Holes are drilled on opposite sides of the underground region to be studied, a transmitter and receiver pair is lowered down these drill holes, and the radio-wave propagation between the pair is recorded. The resulting signals vary according to the electrical properties of the media through which they pass, and from these data we can reconstruct the subsurface structure.

In the cover illustration, the electromagnetic wave transmission is from left to right. The black rectangular area in the center represents a tunnel (the four colored squares within it are calculational artifacts). The two bluish-black horizontal stripes extending to the right from the tunnel's top and bottom are signal minima. In our data-interpretation method for radio-wave probing, these minima determine the tunnel's presence and location. For a description of this subsurface mapping technique and its applications, see the article beginning on p. 11.

ABOUT THE JOURNAL

The Lawrence Livermore Laboratory is operated by the University of California for the United States Energy Research and Development Administration. The Laboratory is one of two nuclear weapons design laboratories in the United States. Today nearly half of our effort is devoted to programs in magnetic and laser fusion energy, biomedical and environmental research, applied energy technology, and other research activities.

The *Energy and Technology Review* is published monthly to report on accomplishments in this energy and environmental research and on unclassified portions of the weapons program. A companion journal, the *Research Monthly*, reports on weapons research and other classified programs. Selected titles from past issues of the *Energy and Technology Review* are listed opposite the inside back cover.

UCRL 52000-77-1
Distribution Category UC-2

January 1977

Energy and Technology Review

Lawrence Livermore Laboratory

Prepared for ERDA under contract No W-7405-Eng-48

BRIEFS

The short items on this page announce recent developments of importance. Some of these items may be amplified in future issues; none of this material is reported elsewhere in this issue.

MAJOR MAGNETIC FUSION EXPERIMENT PLANNED

Funds to start work on our $94 million magnetic fusion test facility (MFTF), the largest mirror device yet, are included in the President's proposed budget. Building on the extremely promising results obtained in the 2XIIB mirror device [see the June 1976 *Energy and Technology Review* (UCRL-52000-76-6), p. 1], this new experiment will explore the major remaining scientific questions surrounding the mirror approach to magnetic fusion energy, beginning in late 1981. The hot, dense plasmas it will investigate will approach those needed for a full-scale fusion reactor.

The MFTF will be appreciably larger than 2XIIB. It will have about 10 times the confinement volume, stand more than 3 times as tall (12 m), and include a 200-tonne superconducting magnet wound with almost 48 km of niobium-titanium filament. This magnet will create the intense field needed to confine 100 trillion plasma particles per cubic centimetre, at 500 million °C, for about 10 ms, perhaps 1% of the confinement time needed for a power-producing fusion reactor.

IMPROVED X-RAY MONOCHROMATOR

We have built a continuously variable x-ray monochromator to measure x-ray detector response more accurately than possible before at LLL. X rays exist over a broad range of energies, and x-ray detectors should, ideally, respond the same to all. Real x-ray detectors fall short of the ideal; they can detect a wide variety of x rays, but they are much more sensitive to some than to others.

Lacking an ideal x-ray detector, the next best approach is to calibrate the response of existing detectors to x rays of different energies. To make such a calibration, we simply expose the detector to known amounts of x rays of a particular energy (monochromatic x rays) and observe the response. There are two problems in this scheme. Natural monochromatic x-ray sources occur only at certain energies, leaving large gaps between. Man-made x-ray sources, however, produce a mixture, not single-energy x rays. The solution is a variable filtering system: one that lets through x rays of only a single energy and discards the rest, but that can be adjusted to different energies to fill in the gaps between natural monochromatic sources.

Our monochromator combines a special collimating system and a flawless crystal of pure germanium. This crystal, represented in the photograph by a lucite dummy, has the special property of passing x rays of only one energy for any given angle of incidence.

Actually, no single monochromator of this design could cover the entire range of x-ray energies that we wanted to observe (15 to 55 keV). Instead, it took three different combinations of crystal thickness and collimation. The highest energy range, from 45 to 55 keV, required the thickest crystal and a collimator 100 mm long with only a 0.5-mm aperture.

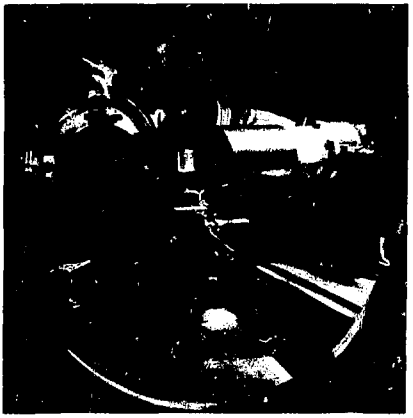

Bragg diffraction x-ray monochromator. Tightly collimated x rays from the source, left, fall on a pure germanium crystal (simulated here with a lucite block) where all but those of a single energy band are absorbed. The transmitted monochromatic x rays then enter the detector, right, where they are counted. Stepping motors below the crystal mounting control the position and orientation of the crystal for "fine tuning" to optimum alignment. The large goniometer (below the x-ray source) controls the angle between the beam of x rays and the front plane of the crystal, thereby determining the energy of the x rays that reach the detector. The overall aim is to determine the energy response function of the detector.

FOSSIL ENERGY

Hoe Creek No. 1: An *In Situ* Coal Gasification Experiment

Gasification in Hoe Creek No. 1, our first *in situ* coal gasification experiment, began on October 15, 1976, and was terminated 11 days later. Twenty-eight hours after ignition, a bypass occurred that channeled most of the burn front to the top of the coal seam. The heating value of the coal did not vary appreciably until near the experiment's termination. We recovered 73% of the energy in the estimated 116 tonnes of coal consumed – 89% of this in the form of combustible gas and the rest as tars. Data gathered indicated good agreement between the experiment and our code predictions in the degree of fracture attained, but showed that spherical high-explosive shots at the coal seam's bottom will not produce a permeability distribution suitable for successful gasification.

Contact Charles B. Thorsness (Ext. 4443) for further information on this article.

Hoe Creek No. 1 was a two-shot experiment whose purpose was to study explosive fracture and gasification. The experiment site is in the Powder River Basin, 32 km southwest of Gillette, Wyoming, in the 8-m-thick subbituminous Felix No. 2 coal seam at a depth of 38 to 46 m. (Site stratigraphy is shown in Fig. 1.)[1] Hoe Creek is a shallow-site coal seam; we expect the perfected gasification technique to be used on deeper resources, coal seams 150 to 1000 m deep.

The experiment was conducted in two phases. Phase 1, in late 1975, included site characterization, fracturing, and preliminary permeability measurements. Phase 2 included detailed fracturing and permeability measurements followed by *in situ* gasification.

In phase 1, one- and two-dimensional computer codes, with compressive shear failure as a criterion, were used to design the actual field test.[2,3] Extensive data on coal mechanical properties were input to the codes, which were normalized with data from laboratory fracture experiments and from an earlier field test at a Kemmerer, Wyoming, coal outcrop.[4]

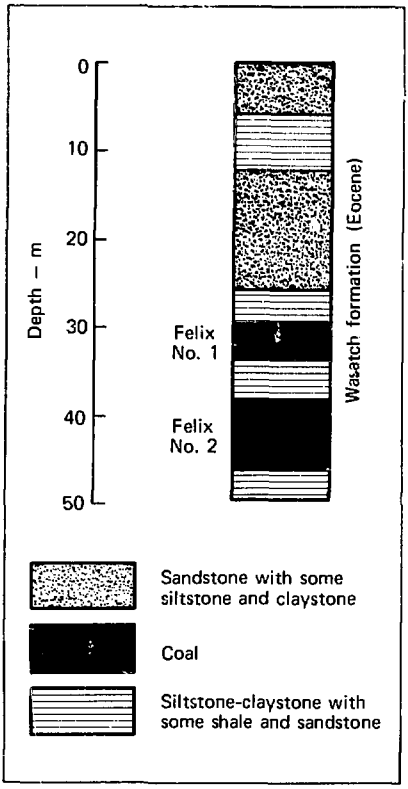

Fig. 1. Hoe Creek site stratigraphy obtained from cores, drill-cutting samples, and downhole geophysical logs. Felix No. 1 and No. 2 refer to coal seams. The top of the 8-m-thick Felix No. 2 seam is at a depth of only 38 m; this is considered a shallow-site bed.

At Hoe Creek, two 340-kg explosive charges were fired simultaneously at a depth of 46 m, the bottom of the coal seam. The explosives were so placed to enhance the permeability at that depth for better liquid drainage and gas flow. Before fracturing, the site geology, hydrology, and permeability were carefully characterized.[5] Postfracture site characterization based on hydrology showed that coal permeability was stimulated from 0.3 μm^2 (0.3 Darcy) preshot to about 2 to 4 μm^2 (2 to 4 Darcy) postshot.[6]

During 1976 we returned to Hoe Creek for phase 2 of the experiment. We redetermined the degree of fracturing, took cores, remeasured the permeability distributions, dewatered the coal, measured air flow, and, finally, gasified the coal.

The final well pattern for phase 2 is shown in Fig. 2. Well I-0 (the original air-injection well) was cased and cemented (outside the casing) down to the top of the coal seam, communicating directly with the rubble-filled HE cavity below it. Well P-1 (the original product-gas retrieval, or production, well) was cased and cemented down to the bottom 2 m of the coal bed. Well I-0 was one of the two HE holes; the other HE hole, marked HE on Fig. 2, was plugged with cement after the shot. Wells I-1 through I-8 were uncased instrument wells containing thermocouples and bubbler tubes for water level measurements and gas sampling. The dewatering wells, DW-1 through DW-6, were steel-cased to the top of the coal and cased with screen through the coal. Each had a 1.6-litre/s-capacity water pump below the seam.

In addition to the wells shown in Fig. 2, there were some core holes in the plan view area, and some environmental wells outside the area. The core holes were fitted with movable thermocouples. Water samples were to be taken periodically from the environmental wells after termination of the experiment to test for possible contamination.

In designing the instrumentation for this experiment, we decided to concentrate on three major measurements:

- Injected-air and retrieved-gas flow rates were measured by orifice flow meters at the I-0 and P-1 wellheads.
- Product gas composition was measured by two on-line gas chromatographs that sampled automatically

at hourly or shorter intervals throughout the experiment.

- Data on the gasification-zone temperature distribution was gathered from thermocouples in all the instrument and dewatering wells.

These measurements and all other data were recorded on strip charts in parallel with a data logger that recorded digitally on magnetic tape.

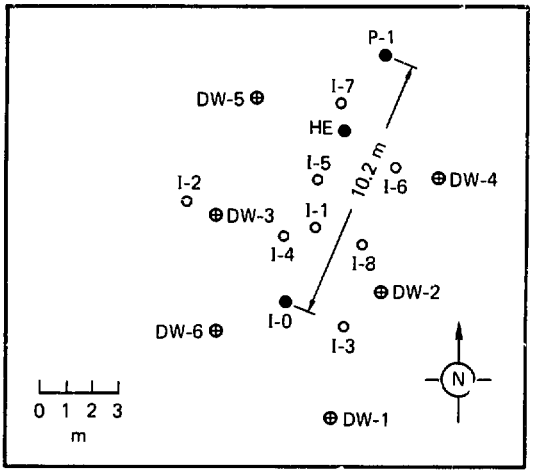

Fig. 2. Plan view of Hoe Creek No. 1 showing bottom hole locations. HE is one of the two shot holes and was plugged to the top with cement before gasification. I-0 is the other shot hole, originally converted to be used as the air-injection well. P-1 is the original gas-production well. After the air-flow tests, we reversed this pattern and made I-0 the gas-production well and P-1 the air-injection well. I-1 through I-8 are instrumentation wells. DW-1 through DW-6 are dewatering wells. Not shown but within the plan view are observation wells and core holes.

Coring and Hydrologic Testing

Postshot examination of cores showed moderate to heavy fracturing in the upper metre or two of the seam, a lesser fractured zone in the middle, and a highly pulverized zone in the bottom 2 to 3 m. Cores from the holes between the two explosive charges showed the most fracturing, cores from the holes farthest out the least. The close correspondence between the postshot degree of fracturing and preshot one- and two-dimensional explosive code calculations has built confidence in our ability to calculate the extent of fracturing. However, from a review of flow behavior pre- and postshot, we've concluded that permeability is not a simple function of the degree of fracturing.

In general, we found that postshot wells completed in the lower part of the seam showed coal of lower permeability than preshot. Well P-1, when initially completed, produced an order of magnitude less water than a nearby preshot well, until extensive cleaning operations finally opened up a connection from it to well I-5.[7]

We made drawdown measurements – essentially, pumping water out of a well and measuring the pressure difference as indicated by the well's water level – in many of the wells. Analysis of these measurements[8] showed three major regions of postshot

permeability: an unenhanced region of 0.3-μm^2 (0.3-Darcy) permeability at distances from the shot of greater than 15 m, a high-permeability (10 to 20 μm^2) inner core region within 3 m of the HE holes, and an intermediate enhanced region (0.5 to 3 μm^2). These permeability values represent averages over the coal thickness.

Other tests, such as slug tests in which water is pumped into a well and the water level monitored, showed similar permeability patterns but also indicated a considerable degree of heterogeneity in these three regions.

From the hydrology and coring data we conclude that the explosive-charge fracturing enhanced the average permeability in the vicinity of the charges, when the seam is viewed in a two-dimensional aerial perspective. When viewed in cross section, however, postshot permeability is less than preshot levels at certain vertical locations near these charges. We believe this to be a result of plugging by coal fines produced by the intense close-in fracturing. Consequently, although the explosives were emplaced at the bottom of the coal bed, much of the permeability enhancement tended to be near the seam's top.

Dewatering

Dewatering rates were in good agreement with estimates.[9] After a few hours of higher flow rates, a relatively constant rate of water withdrawal of approximately 0.6 litre/s for the entire experiment area was observed. This withdrawal rate was maintained until pressurization during air-flow tests cut the rate to near zero.

Wells DW-1 through DW-6 and P-1 (Fig. 2) were pumped below the coal seam bottom. The water level in I-5, I-7, and the HE well dropped to within a few metres of the bottom within 1 hour. However, the level in one of the observation wells only a few metres away from P-1 remained well above the top of the coal, indicating the local variation in permeability.

Air-Flow Tests

Air-flow tests were begun by injecting air into well I-0 at a gauge pressure of about 100 kPa (15 psi). The pressure was gradually raised to about 400 kPa and the flow allowed to stabilize. No leakage to the surface was observed, but gauge pressures of up to 30 kPa were observed in wells 30 m away. Air losses to the underground system were approximately 40% for this mode of operation. Because the I-0 well had been cased only to the top of the coal seam, injecting air into it put high pressure on the entire cavity and led to many possible paths for leaks to the surrounding formation.

Reversing the air flow and injecting into well P-1, which had been cased through the coal seam, put high pressure at the seam's bottom. This reduced the pressure in the I-0 well and also reduced the air losses. About 95% of the injected air was recovered in this mode of operation.

Because of the large air loss found when injecting in I-0, we decided to reverse our original intention and gasify from well P-1 to well I-0. P-1 therefore became the air-injection well and I-0 the gas-production well.

Two sulfur hexafluoride tracer runs were made, one for each flow direction. We injected the sulfur hexafluoride and air, timing the tracer's appearance and measuring its concentration at the gas-production well. From these quite successful tests, we calculated an accessible void volume in the seam of about 20 m^3.

Gasification

Ignition. We used electrical resistance heating (1 kW) to ignite the coal. Two electric barbecue charcoal lighters were strapped together and lowered down the P-1 well along with a thermocouple. Several bags of charcoal briquets were dumped down the well until the lighters were covered. Once all valves were properly set and the air flow turned on, the charcoal ignited in a few minutes, as indicated by the thermocouple. Ignition took place at 16:30 on October 15, 1976 (day 289.7, day 0 being midnight on December 31, 1975). The injection and production flow rates are shown in Fig. 3 for the entire experiment.

History. As mentioned previously, a good communication path was established through the bottom part of the coal seam between wells P-1 and I-5, in the center of the gasification zone. We expected that the burn would progress along this path and then

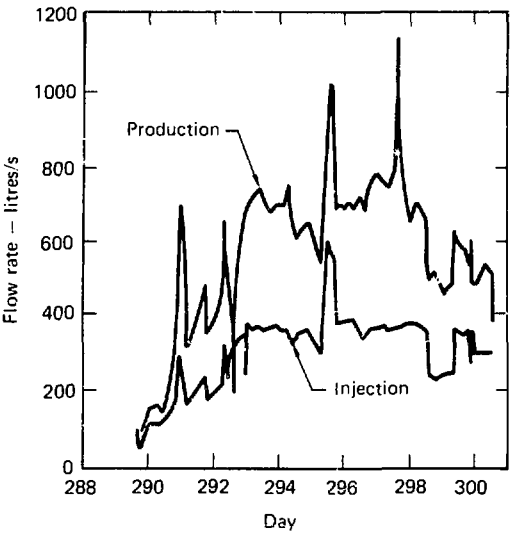

Fig. 3. Air-injection and gas-production flow rates for the entire gasification experiment. (Ignition took place on day 289.7, day 0 being midnight on December 31, 1975.) Production flow was calculated from a nitrogen balance – comparing the percentage of nitrogen in the injected air to its percentage in the recovered product gas (nitrogen does not enter into the gasification reaction) – from day 291.4 to day 292.2.

travel upward and go along the top of the seam to well I-0. At first this seemed to be the case. With an input gauge pressure of about 400 kPa, the gas output flow dropped from 61 to 50 litres/s during the first 2 hours after ignition, and then rose steadily for the rest of the day. Thermocouples in wells I-7 and I-5 responded within 1 hour of ignition. Temperatures of about 100°C were recorded at the 43-m level, two-thirds of the way into the coal seam, at both wells.

On the second day of gasification (day 290) temperatures began to rise in wells I-1, I-6, I-8, and DW-4. At about day 290.6 we had a channel bypass: the burn front moved mostly to the top of the seam. The output flow increased sharply to 610 litres/s and a large quantity of water was produced. We lowered the injection pressure several times to control the flow, but after a few hours of controlled production the flow increased suddenly to over 1100 litres/s accompanied by the emission of coal fines mixed with tar. All of the pressure and gas sampling lines were quickly plugged as well as the production flow meter orifice plate. The bypass line around the flow meter section was opened to shunt the gas flow while repairs were made.

The heating value of the produced gas is shown in Fig. 4. A slight but steady decline in the days following the bypass at day 290.6 is evident.

A high-flow test (almost doubling the air-injection rate) was run on day 295.5 (see Fig. 3). The heating value of the gas did not change appreciably (Fig. 4) nor were major changes in temperature noted during this test. For a time, we also injected water into well P-1 at a rate of 0.06 to 0.1 litre/s – a rate that injected an amount almost equal to the natural influx.

No measurable effect on any parameter was found, further evidence that the burn was near the top of the coal seam at this time.

By day 297 the burn front was close enough to the production well, I-0, so that the ouput gas temperature had reached 400°C and was still climbing. A small leak had developed in the grout seal around the well casing, and the valve gaskets were being seriously overheated. We made an attempt to cool the gas by flooding wells DW-1 and DW-6. Although a slight decrease in wellhead temperature was noted, the main effect was to increase the production gas flow rate and cause a momentary increase in heating value to 5.6 MJ/m^3 (150 Btu/ft^3). This caused the flare stack temperature to climb, so we stopped the cooling attempt and turned the pumps back on.

Reducing the flow rate by cutting the input pressure helped to reduce the output temperature, but it also caused a serious deterioration in the heating value of the gas. Raising the pressure did not restore the heating value to its original point, and the deterioration continued. We shut the compressor down and terminated the gasification experiment on day 300.

Results. Gasification proceeded for 11 days. During this time approximately 280 000 m^3 of air were injected and 530 000 m^3 (370 000 m^3 dry) of gas were produced. Initial air-injection absolute pressure was approximately 500 kPa, which fell rapidly on the second day of operation to a value of 170 to 200 kPa. Production pressures were generally about 30 kPa lower. This rapid decrease was a result of the rapid increase in flow conductance of the formation.

Just after ignition the relative conductance fell rapidly and then recovered to approximately 70% of its pregasification level. It maintained this level for about half a day. A rapid rise then occurred, and during the course of the remainder of the gasification (which was most of the gasification period), conductance was 50 to 100 times its pregasification value.

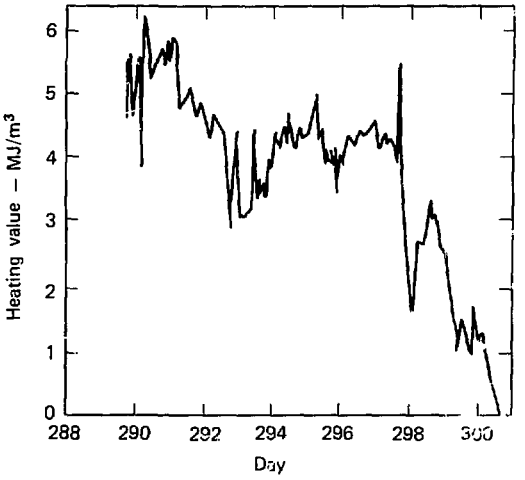

Fig. 4. Dry-gas heating value during gasification. Even though there was a steady decline following the channel bypass at day 290.6, the heating value did not change appreciably until near the end of the experiment.

Gas losses during gasification were only significant during the early high-pressure operations. We ultimately recovered 93% of the nitrogen present in the injected air. Since nitrogen does not enter into the gasification reaction, we used it to monitor gas losses.

We measured the dry gas composition for its primary components nitrogen, hydrogen, carbon monoxide, carbon dioxide, and methane with a gas chromatograph. During the first two days of the test, a higher percentage of pyrolysis gases were present, resulting in a higher methane concentration. During the central portion of the tests, gas composition was relatively stable. Near the end, as the oxidation zone approached the exhaust well, carbon monoxide, hydrogen, and methane levels declined markedly. We found no evidence that the high-flow test had influenced gas composition. However, a definite change in the composition is indicated during and after the injection of the water slug on day 297 -- a rapid rise in hydrogen concentration followed by a rapid decline in carbon monoxide, hydrogen, and methane. This gas composition change was apparently caused by the added water slug and would not have resulted from the continued normal water influx alone.

Considerable quantities of water were produced in the form of liquid and gas during the gasification test. Liquid water was produced by pumps located in the dewatering wells; steam was produced from the gasification production well. This steam accounted for 30% of the total produced-gas volume (see Fig. 5).

The burn geometry as deduced from the thermocouple data and coal consumption estimates is shown in Fig. 6. The burn started at the bottom of well P-1 and, until the channel bypass, progressed horizontally towards well I-5 and also vertically towards the seam's top. After the bypass, the burn went mostly along the top of the seam, but also continued along the central line at a lower elevation.

The total energy recovery in the form of combustible gas was 65% of that available from the estimated 116 tonnes of consumed coal. Figure 7 shows the total energy balance. Note that if the combustion energy estimated to be present in the produced tars is included as usable energy, the total useful energy recovery becomes about 73% of the consumed coal. The underground losses of heat energy were quite small, the largest energy loss from the system was in the considerable production of steam.

Conclusions

Explosive Fracturing. Hoe Creek experiment No. 1 is probably one of the most thoroughly diagnosed fracture experiments ever performed by the Laboratory. The general agreement between the experiment and our one- and two-dimensional code predictions is quite good. But there are still some details that are not clear. The layered appearance of the fracturing and the rather large-scale asymmetries as a function of height from the shot points are hard to understand in what appears to be a very homogeneous coal seam.

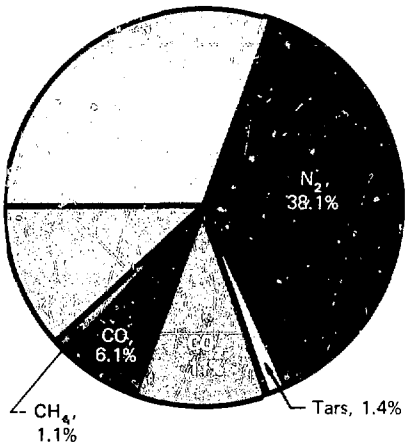

Fig. 5. Major gas product distribution on a mole basis.

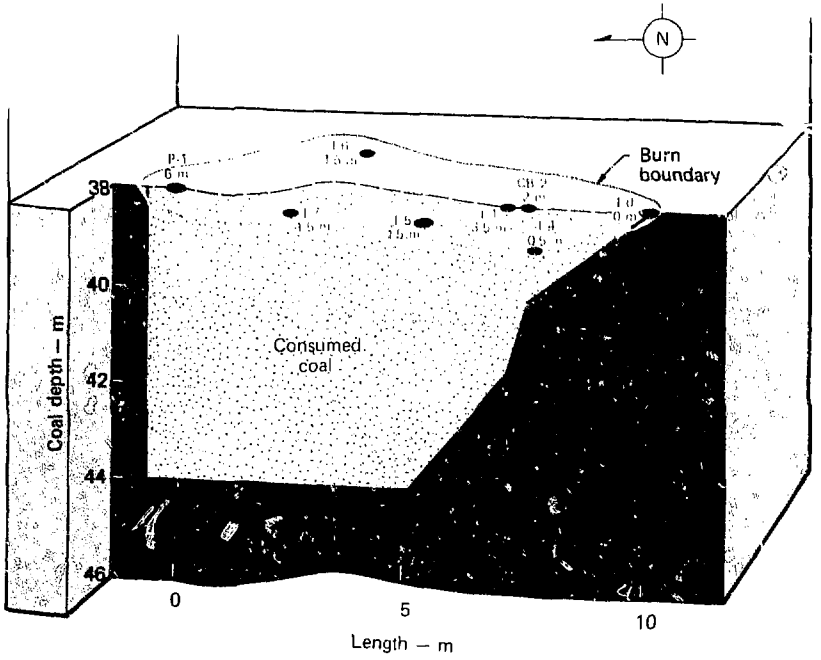

Fig. 6. Plan view (yellowish area) superimposed on cross section of the Hoe Creek No. 1 gasified volume as estimated from temperature measurements. P-1 was the air injection well. I-1, I-4, I-5, I-6, and I-7 are instrument wells. CB-2 is a core hole. The depths cited next to the well callouts are burn depths at those wells.

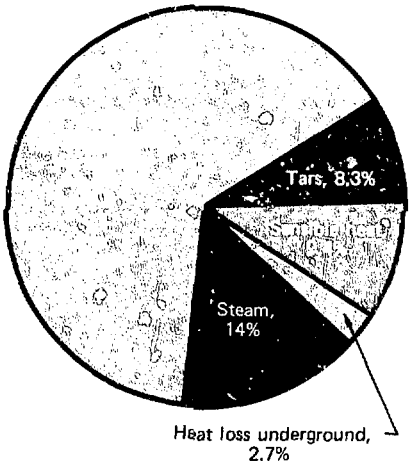

Fig. 7. Energy distribution in the gasification as a percent of consumed coal energy. The total energy recovered in combustible gas was 65% of that available from the estimated 116 tonnes of consumed coal. (Sensible heat is that heat given off by the product gas as it returns to ambient temperature.)

Our knowledge of the relationship between degree of fracture and permeability is even less satisfactory. In fact, comparing the results from the Kemmerer and Hoe Creek experiments, it is obvious that total failure strain (shear plus tensile) is not a reliable predictor of permeability. We are looking into the possibility that tensile failure[10] may be more directly related to permeability.

The results from Hoe Creek No. 1 indicate that spherical HE shots placed at the bottom of the coal seam did not produce a permeability distribution suitable for gasification. We are considering other geometries and types of explosive for future experiments.

Gasification. Forward combustion gasification was achieved without any problem of formation plugging. After two days of operation, flow conductivity was an order of magnitude above pregasification levels. However, even before this channel bypass condition was reached, plugging did not seem to be serious.

The bypass of the flow that occurred after 28 hours of gasification limited the total volume of coal gasified.

The gas composition, gas heating value, and oxygen utilization were all fairly constant during the course of the burn. Marked change occurred only at the end of the experiment. Gas composition was not influenced by doubling the air injection rate.

The total water influx into the gasification region was about 65% of the pregasification level, and about 30% of this amount entered the hot zone. This water influx did not appear to influence product-gas composition, however, indicating that it mixed with the hot gas after the reactions were completed. Still, the influx of water into the system may have limited the amount of coal recovered by limiting the lateral spreading of the burn zone.

Energy recovery in the form of combustible products amounted to 75% of the energy in the consumed coal. There were essentially no losses to the subsurface formation; the greatest energy loss was in the production of steam.

Key Words: Hoe Creek Project; coal gasification; coal – fracturing; formation fracturing, coal – permeability.

Notes and References

1. *LLL* In Situ *Coal Gasification Program, Quarterly Progress Report, July through September 1975*, Lawrence Livermore Laboratory, Rept. UCRL-50026-75-3 (1975).
2. An overview of the LLL *in situ* coal gasification program is given in the April 1975 *Energy and Technology Review* (UCRL-52000-75-4), p. 8; phase 1 of the first Hoe Creek experiment is briefly described in the November 1975 *Energy and Technology Review* (UCRL-52000-75-11), p. ii.
3. D. Stephens, F. Beane, and R. Hill, *LLL* In Situ *Coal Gasification Program*, Lawrence Livermore Laboratory, Rept. UCRL-78308 (1976); also in *Proceedings of the 2nd Underground Coal Gasification Symposium, Morgantown, W. Va., August 1976.*

4. J. Hearst, T. Butkovich, E. Laine, R. Lake, D. Leach, J. Lytle, J. Sherman, D. Snoeberger, and R. Quong, "Fractures Induced by a Contained Explosion in Kemmerer Coal," *Int. J. Rock Mech. Min. Sci. & Geomech. Abstr.* 13, 37 (1976).
5. R. Stone and D. Snoeberger, *Evaluation of the Native Hydraulic Characteristics of the Felix Coal (Eocene, Wasatch Formation) and Associated Strata, Hoe Creek Site, Campbell County, Wyoming*, Lawrence Livermore Laboratory, Rept. UCRL-51992 (1976).
6. *LLL* In Situ *Coal Gasification Program, Quarterly* Progress Report, October *through December 1975*, Lawrence Livermore Laboratory, Rept. UCRL-50026-75-4 (1976).
7. *LLL* In Situ *Coal Gasification Program, Quarterly Progress Report, July through September 1976*, Lawrence Livermore Laboratory, Rept. UCRL-50026-76-3 (1976).
8. D. Snoeberger, *Field hydrological Tests of Explosively Fractured Coal*, Lawrence Livermore Laboratory, Rept. UCRL-78957 (1977).
9. *LLL* In Situ *Coal Gasification Program, Quarterly Progress Report, April through June 1976*, Lawrence Livermore Laboratory, Rept UCRL-50026-76-2 (1976).
10. T. Butkovich, *Calculation of Fracture and Permeability Enhancement from Underground Explosions in Coal*, Lawrence Livermore Laboratory, Rept. UCRL-77945 (1976).

ENGINEERING RESEARCH

Mapping Underground Structure With Radio Waves

We have developed mapping techniques for determining subsurface structure from radio-wave transmissions. Transmitter and receiver pairs are lowered in holes drilled on opposite sides of the underground region to be probed. The signature of the electromagnetic waves propagated between these pairs varies according to the electrical properties of the intervening media. From this signature we can locate anomalies in the electrical properties of the intervening media; in many cases, these anomalies can be directly related to geologic structure. Such radio-wave probing has a variety of possible applications, including assessing underground sites for nuclear reactors or urban transit stations, locating tunnels or water-bearing strata, and mapping the burn front for *in situ* coal gasification.

Is it possible to know what exists beneath the ground before you dig it up? With the electrical methods for probing subsurface electrical structures being developed and tested at LLL, the answer is yes. Our approach has been to adapt the data-collection and -interpretation procedures that are being applied in medical diagnostics (e.g., brain and whole-body scans) to probing the ground with radio waves. We map the region of interest with electrical signals transmitted between transmitter and receiver pairs lowered in boreholes on opposite sides of the region. The signals so produced vary according to the electrical properties of the media through which they pass; from their signature we can reconstruct the subsurface structure, identifying anomalies, water-bearing strata, sand lenses, and the like.

Early experiments have led to radio-wave probing techniques with good resolution when the subsurface region is relatively homogeneous and the electrical contrast between the host medium and the anomaly of interest is small.[1] Probe separations can be from 30 m to 1 km, depending on the media involved. We have used these techniques, for example, to determine the fracturing pattern induced in a coal seam by detonating high explosives. The dominant propagation mechanism from transmitter to receiver through this fractured coal medium is easily and adequately described by straight-line ray optics.

More recently, we extended our studies to include locating high-contrast anomalies in the host medium,

Contact R. Jeff Lytle (Ext. 8214) for further information on this article.

i.e., anomalies with significantly different electrical propagation characteristics from the host medium. In two experiments we used high-frequency electromagnetic waves propagated between boreholes to locate a tunnel in granite. In these experiments, funded by the Advanced Research Projects Agency, we found the dominant interaction mechanism to be diffraction. To help us interpret the experimental data, we also began theoretical modeling to describe this interaction more fully.

Locating high-contrast underground anomalies like voids, water pockets, or abandoned tunnels can be difficult if the anomaly is deep beneath the surface. This difficulty is compounded if one is limited to measurements from the surface or from a single borehole. Locating such subsurface structures is important, however, when scheduling excavating equipment. For example, in urban tunneling for underground transit systems, equipment costs are high. Expenses mount rapidly when equipment to cut granite stands idle while the tunnelers remove gravel from an unsuspected subterranean stream bed, or while different tunneling equipment is brought in to remove an unexpected clay seam. Electrical mapping is a sensible alternative to the conventional practice of punching test holes at 15-m intervals along the transit route and then inferring the intervening geology.

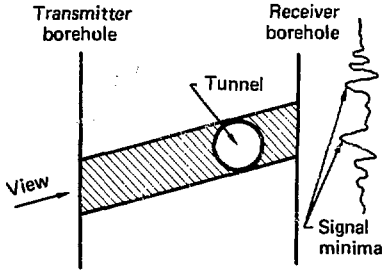

Fig. 1. Back-projecting signal minima to locate an underground tunnel. We lower a transmitter and receiver pair down boreholes drilled on opposite sides of the host medium and record data at a number of fixed depths. (An offset pair is shown here; the transmitter is kept a fixed interval deeper in its borehole than the receiver.) The two strongest adjacent minima in the received signal define the sector of the host medium in which the tunnel should be located. Superimposing a series of these views taken at different depths and transmitter/receiver orientations allows us to determine the tunnel's location.

Theoretical Modeling

In our theoretical modeling work, funded by the U.S. Department of Transportation, we considered the effect of tunnel shape on the electromagnetic field.[2] Interaction with tunnels shaped as right circular cylinders yields to an exact mathematical solution in terms of sums of Bessel functions. Interaction with tunnels of arbitrary shape can be modeled by an approximate integral-equation approach. The basic experiment modeled consisted of physically and electrically small electric dipole transmitters and receivers oriented vertically in separate boreholes on either side of the tunnel. We assumed that the tunnels run nearly parallel to the earth's surface and that the boreholes and tunnel are deep enough for electromagnetic interaction with the surface to be negligible.

We considered two cases: lowering transmitter and receiver pairs at the same depth in unison past the tunnel region, and lowering the pairs in unison with fixed differences in their depths. In both cases, we noted an oscillating signal with deep minima near the tunnel. These signal minima were centered about the projected middle of the tunnel, which suggested a useful diagnostic: the two strongest adjacent minima define the most probable sector containing the tunnel. Simultaneously lowering a transmitter and receiver held at equal depths provides a horizontal view of the anomaly. Other views are obtained by lowering a transmitter and receiver offset by a fixed distance. By recording data at a number of depths in the borehole, drawing sectors from their minima, and then superimposing these sectors (or views) as in medical back-projection (see below), we could estimate the tunnel's location (Fig. 1).

Figure 2 shows the calculated signal minima located above and below the tunnel on the transmission side

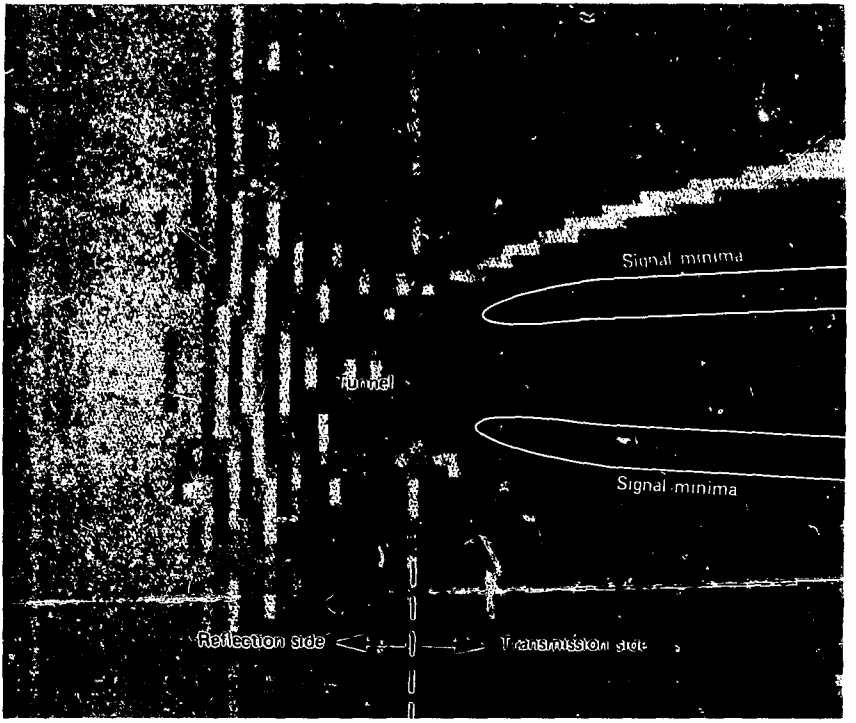

Fig. 2. Calculated radio-wave transmission past a realistically shaped tunnel. The incident plane wave here is moving from left to right. Two distinct signal minima are produced on the transmission side of the tunnel. In the calculation, they were still evident some 30 m beyond the tunnel's center. Our data-interpretation method for cross-borehole radio-wave probing is based on the location of these two minima.

of a realistically shaped tunnel. Because of the voluminous amount generated, we displayed the data as shading. The minima – almost black horizontal stripes – are quite distinct; in the calculation, they were still evident 30 m beyond the tunnel's center.

The excitation frequency in Fig. 2 was 57 MHz. The effect of varying frequency was most evident in the width between successive maxima and minima. Going to higher frequencies gave better detail, but lower frequency signals propagate farther. For our calculations, we selected frequencies from 10 to 80 MHz. Below about 20 MHz, we found that signal variation was generally insufficient to allow confident interpretation of a tunnel's location in the presence of small-scale geologic noise. Between 25 and 60 MHz, resolution was adequate. Above 60 MHz, the data varied too rapidly for successful analysis with the simple data-interpretation method.

Defining views of the tunnel from just the two signal minima is a modification of the classical back-projection technique used in medical diagnostics, wherein features inside the body show up as anomalies in the data when scanned by a transmitter/receiver pair. We also used a classical back-projection algorithm like those applied to interpret multiview medical x-ray data from brain or tumor scans, in which the complete signature is used. Figure 3 shows such a profile calculated for the complete region between boreholes. The darkest area again represents the tunnel, but it is not so well defined as in Fig. 2. Also, the surrounding shadings are artifacts of the calculation and do not adequately represent the homogeneous region external to the tunnel.

We have initially concentrated, therefore, on applying our *modified* back-projection technique to interpret experimental data for the location of anomalies. However, profiles of the complete region around an anomaly could be useful, and improving their resolution is one of our future goals.

Field Experiments

One of the advantages of our modified back-projection technique is that it permits easy and rapid interpretation of data in the field. No computers or even calculators are required to determine a tunnel's location. The solution is easily obtained graphically.

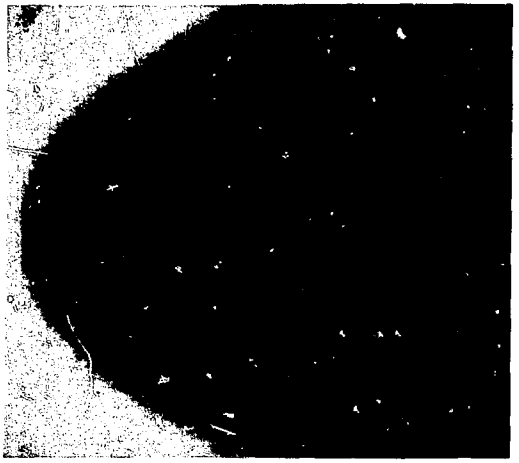

Fig. 3. Calculated profile for the complete region between two borehole probes, derived from classical back-projection. Although the tunnel is again evident (the darkest region), it is not so well defined as with our modified back-projection technique. We are working to improve the resolution of this algorithm.

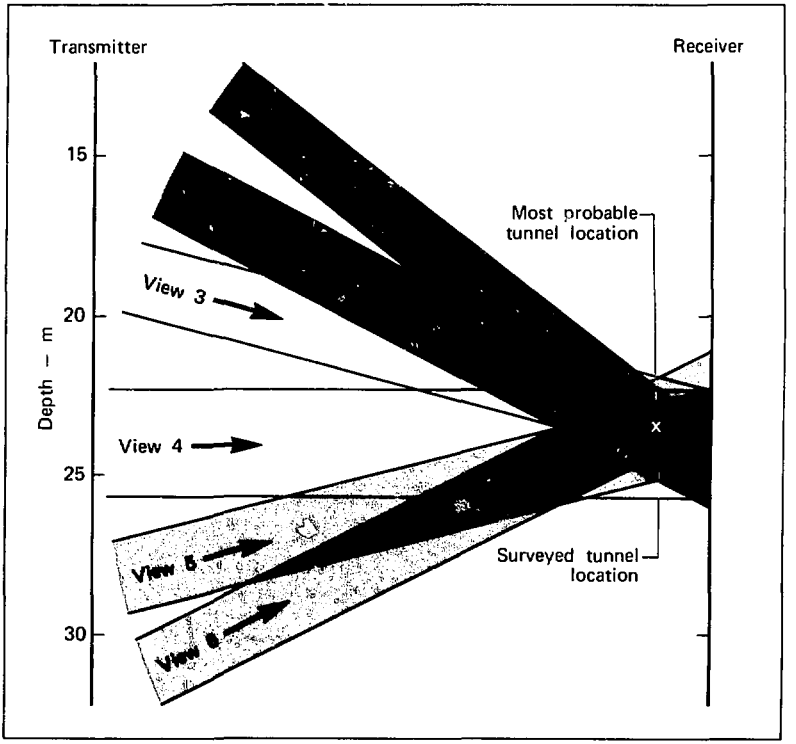

Fig. 4. Data record from the Gold Hill experiment. The six views here were made at 57 MHz, with a transmitter-to-receiver borehole separation of 20 m. Superimposing these views gave us a most-probable tunnel location that was within 1 m of the tunnel's surveyed position.

Our first experiment was at the Bureau of Mines test area near Gold Hill, Colorado. The area has a tunnel passing through granite with four drill holes nearby suitable for our probes. Drill-hole depth varies from 30 to 60 m; the 1.5-m wide tunnel is located between the 23- and 26-m depths. Depending on the holes used, signal transmissions covered from 20 to 25 m.

We recorded data at 0.6-m intervals in the drill holes at frequencies of 25, 57, and 80 MHz. Detailed data were taken for a number of views at each frequency. The six views at 57 MHz for a transmitter-to-receiver borehole spacing of 20 m are shown in Fig. 4. Because of the large amount of data gathered, the tunnel's existence was confirmed and its region reasonably well defined. The center of the most-probable tunnel location is within 1 m of the tunnel's surveyed center.

A limited amount of data was also recorded for a probe separation of 25 m at 57 MHz. Again, accuracy was reasonably good. The most-probable tunnel depth was correct within 0.6 m; horizontally, we were within 2 m of the tunnel's center (though working from only three views).

We concluded that the presence of a tunnel or cavity as well as its horizontal and vertical location can be determined with cross-borehole, continuous-wave, electromagnetic transmission. The physical mechanism governing this signal transmission appears to be similar to the characteristic Fresnel diffraction from a metallic strip. One possible explanation is that the high electrical contrast of the tunnel with the surrounding medium makes the tunnel behave like the metallic strip. We also noted that typically the signal on the transmission side of the tunnel (i.e., on the other side of the tunnel from the transmitter) is more varied – and thus easier to interpret in the presence of geologic noise – than on the reflection side.

A similar experiment conducted near China Lake, California, produced comparable results. A new adit for a tungsten mine was being drilled, and we performed cross-borehole transmissions before and after the tunnel passed by our boreholes. We drilled three holes, with 26 m separating the two extremes. Our recording setup is shown in the photograph of Fig. 5; the transmitter was lowered in the background borehole, receivers were lowered in the two foreground holes.

Having noted the rapid variation of signal with depth in the Gold Hill experiments, we recorded data at 0.3-m intervals this time. The signature of the horizontal view after drilling contained two deep minima (Fig. 5) not present in the "before" signature.

An interesting sidelight of this experiment was that by monitoring the deep minima, we could see a rubble cart passing through the tunnel. As the cart passed by our line of boreholes, the signal minima would oscillate. The behavior of this variation indicated that the electrical waves probed more than just the narrow plane between the two boreholes; one would expect them to probe an elliptical region, with the boreholes at the foci of the ellipse.

Future Directions

As a result of the work cited above, data interpretation is now possible for cross-borehole electromagnetic probing of geologic media with either high- or low-contrast anomalies. Because the data signatures of these two situations – governed by diffraction vs straight-line ray optics – are clearly different, it is evident which interpretation algorithm applies. So far, however, we have only applied these algorithms to data obtained at relatively clean (homogeneous) geologic sites. The effects of a more complex medium on data signatures still needs to be explored. For example, the masking of one moderate-contrast anomaly by another may create problems in an inhomogeneous medium. We are developing a technique (governed by refraction) more suited to such media.

Numerous investigators have used pulsed signals to probe media for their structure. Pulsed probing is usually done with a reflection rather than a transmission signal, and little data processing is needed in presenting data so gathered. The received signal is simply displayed as a function of time for a number of transmitter and receiver positions. The interpretation of such data is generally claimed to be obvious even to the untrained observer. In preliminary tests, however, we have found that swept-frequency measurements with a data display similar to the pulsed

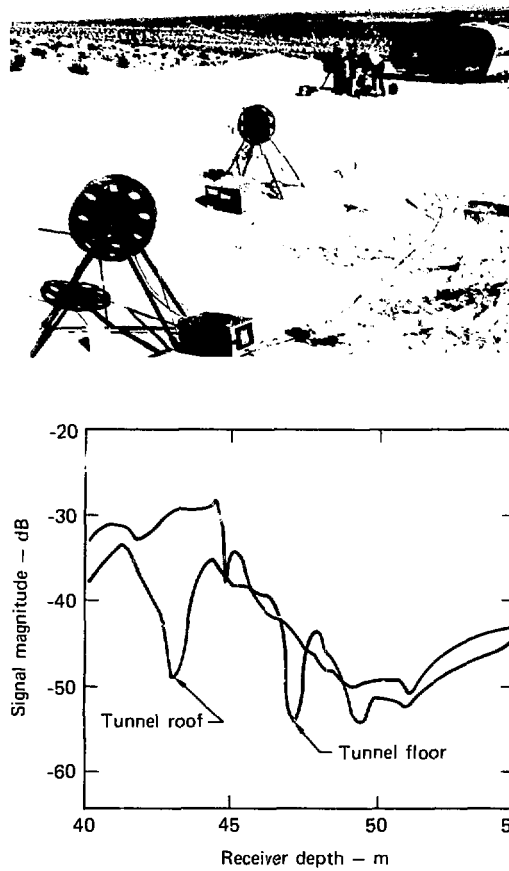

Fig. 5. Experimental setup (top) and data record (bottom) of our "before" and "after" transmissions near China Lake, California. We drilled three boreholes: receivers were lowered in the two foreground holes, a transmitter was lowered in the background hole. The deep signal minima in the data recorded after the tungsten mine was drilled through (colored curve) show the tunnel roof and floor. Both minima are absent from our "before" record (black curve). The signal levels indicated are relative to 1 mW.

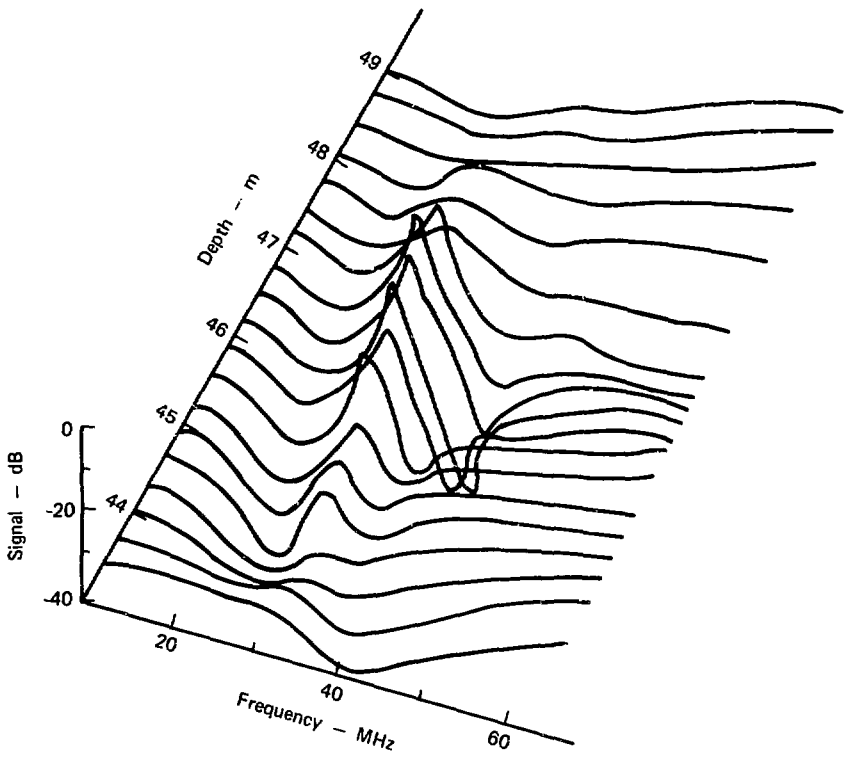

Fig. 6. Data record from swept-frequency cross-borehole probing at our China Lake experimental site. The advantage to this measurement technique is the clarity with which an anomaly – here the floor of the tungsten mine – can be displayed.

probing technique make the locations of significant anomalies equally or even more evident.

Recording data over a frequency sweep – say from 10 to 60 MHz – has several advantages compared with pulsed probing. The effects of dispersion (pulse broadening) are not encountered with a continuous wave signal. In addition, pulsed probing requires higher frequencies and higher power than are typically needed to resolve an anomaly. With lower-frequency continuous waves, the attenuation is less and the signal will propagate farther. This enables one to space boreholes more widely and still maintain adequate resolution. We tested swept-frequency cross-borehole probing

during our China Lake experiment. As shown in Fig. 6, the tunnel's presence is clearly evident.

Finally, we are also examining methods for interpreting signals obtained from a single borehole rather than from cross-borehole transmissions. For example, we are designing a directional antenna to fit into a 15-cm-diameter borehole. Besides its size advantage, this antenna will eliminate the ambiguity that arises with conventional antennas in interpreting reflection data from a single borehole. Unlike conventional antennas, which have no azimuthal discrimination, our directional antenna will allow us to infer the direction from which signals are reflected. We are now completing the theoretical design of this antenna and have plans for building one in the future.

Key Words: electromagnetic waves – applications; electromagnetic waves – mathematical analysis; electromagnetic waves – propagation.

Notes and References

1. This early work is described in the January 1976 *Energy and Technology Review* (UCRL-52000-76-1), p. 10.
2. For a more detailed discussion of the theoretical modeling studies, see J. Lytle, D. Lager, E. Laine, and D. Davis, *Using Cross-Borehole Electromagnetic Probing to Locate a Tunnel*, Lawrence Livermore Laboratory, Rept. UCRL-52166 (1976).

PHYSICAL SCIENCES

Measuring Hydrogen-Isotope Distribution Profiles

We have developed a new nondestructive technique for measuring the depth distribution of hydrogen isotopes absorbed or implanted near the surface of any material. The method allows real-time study of the inventory and diffusion of hydrogen, deuterium, and tritium. Briefly, the technique involves bombarding the surface with a monoenergetic beam of ions chosen for their ability to react with the hydrogen isotope in question, producing fast neutrons. The energy distribution of the neutrons is a sensitive indicator of the energy of the bombarding particles at the instant of reaction, and hence of the depth of the reaction sites below the surface of the material. We have obtained a sensitivity of one part per million for tritium in copper. We are applying the technique to several energy-related materials problems.

Some materials, among them titanium, scandium, erbium, and uranium, have an affinity for hydrogen and its heavier isotopes, deuterium and tritium. This affinity can be an advantage, as in the fabrication of titanium-tritide (TiT_2) targets for neutron production. In other cases it can be a serious disadvantage. Steel, for example, loses as much as 50% of its ductility on absorbing hydrogen, limiting its usefulness in the coal gasification program.

The inside walls of fusion reactors will be bombarded by deuterium and tritium ions, which will accumulate below the wall surfaces. In some materials, absorbed hydrogen migrates away after such implantation; in others it may stay in place. Exactly how the hydrogen moves with respect to changes in temperature, past history, radiation damage, chemical composition, and preloading with hydrogen, and how the presence of hydrogen isotopes affects such properties as strength and ductility, are of great importance to fusion reactor research as well as to our *nuclear explosives programs.*

We have developed a fast, sensitive, nondestructive method for measuring concentrations of hydrogen isotopes in solid materials, a method that should have wide applications. It is based on measuring the energy spectrum of neutrons produced when we bombard a hydrogen-loaded material with a beam of energetic ions. At a well-defined energy, the reaction between protons and tritons (hydrogen and tritium nuclei), for

Contact Carl H. Poppe (Ext. 8944) for further information on this article.

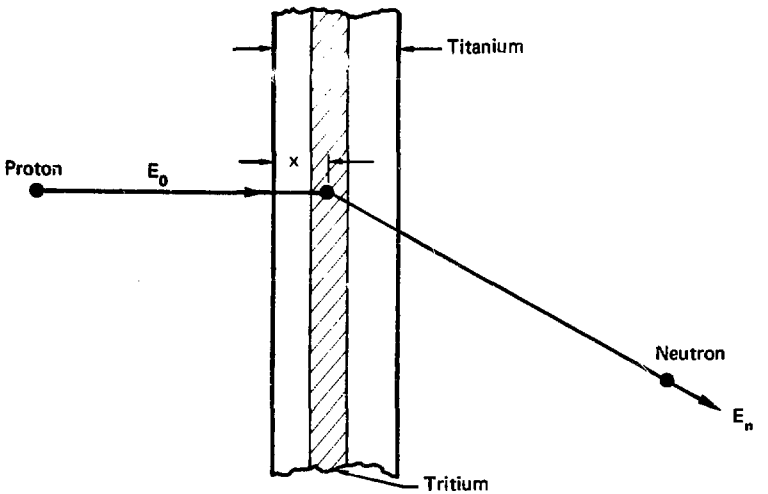

Fig. 1. Schematic representation of a tritium depth-profiling measurement. Protons with an initial energy E_0 interact with tritium embedded in a titanium matrix, liberating neutrons. The energy of each neutron depends on the energy of the proton that liberated it, and this in turn depends on the distance x that the proton penetrated before encountering a tritium atom. Hence measuring the neutron energy yields information about the tritium distribution with depth.

example, produces large numbers of monoenergetic neutrons. Only in those reactions that take place right on the surface can the bombarding particles have their full energy, however. As the bombarding particles penetrate below the surface, they lose energy, and this energy loss affects the energy of any neutrons they produce. Conversely, measuring neutron energy defines the energy of the particle that caused the reaction, and hence the depth in the material where the reaction took place. Measuring how many neutrons there are for each particular energy range gives us an indication of how many hydrogen nuclei were available at each depth in the material. We call this concentration vs depth a hydrogen-isotope profile.

Figure 1 outlines this process in more detail for tritium depth profiling. A beam of protons of well-defined energy E_0, produced in an accelerator, bombards a metallic titanium target in which there is an unknown concentration of tritium at some distance below the surface. As each proton enters the titanium it begins to lose energy; in fact, the amount of energy it loses is roughly proportional to the depth as it penetrates. When the proton encounters the tritium-filled region, it has a definite probability of reacting with a tritium nucleus at some depth x and producing a neutron. This interaction probability depends on the nuclear reaction cross section (a measured, known quantity) and on the concentration

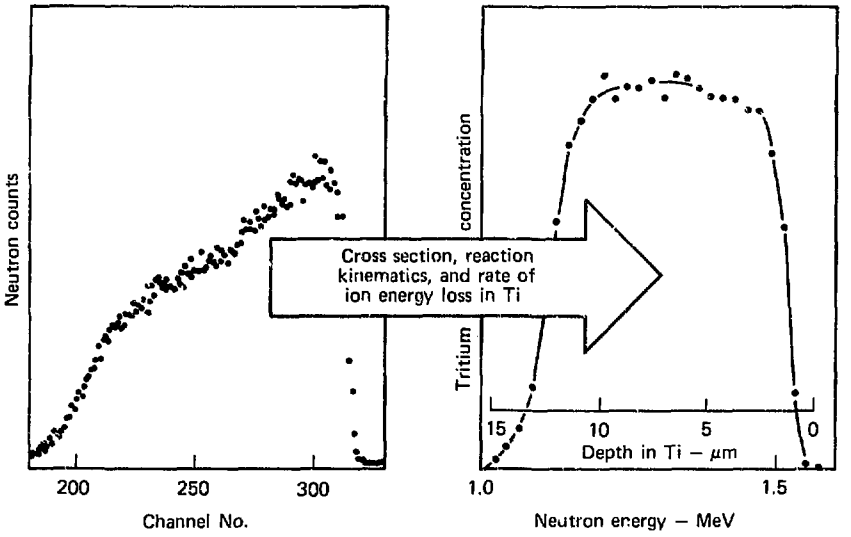

Fig. 2. A neutron velocity spectrum (left) and the tritium concentration profile that can be calculated from it (right), given the reaction cross section, the reaction kinematics, and the energy loss rate of protons in titanium.

of tritium atoms (unknown). Although a neutron might also come from a proton hitting a titanium atom, the probability of this reaction is relatively insignificant.

The neutron's energy depends in part on the energy of the incident proton, and this in turn depends on the initial energy of the beam and the energy lost in penetrating to the depth x where the neutron was produced. Neutron energy, and hence its flight velocity, is independent of how thick the rest of the target is. Because of its lack of charge, the neutron leaves the target without losing energy.

When a large number of neutron velocity measurements are accumulated, we sort them and display the result as a neutron velocity spectrum (Fig. 2). Knowing the nuclear cross section, the kinematics of the reaction, and how the proton slows down as it goes through the target, we can program a computer to convert this velocity spectrum into a map of tritium concentration vs depth.

This technique will work with any neutron-producing charged-particle reaction. To map a hydrogen concentration, we bombard with tritium ions. To map a deuterium concentration, we bombard with deuterons. For a lithium concentration, we can bombard with protons, producing neutrons by the ^{7}Li(p,n) reaction.

Figure 3 is a schematic layout of our experimental apparatus. The pulsed ion source produces bunches of protons, deuterons, or tritons, as required. The ion bunches, typically about 1 ns in duration and coming every 200 to 500 ns, are accelerated to several million electron volts in the Cyclograaff tandem accelerator. A magnet sorts the ions according to momentum,

passing only those of a precisely defined energy. A feedback loop enables us to regulate beam energy to a precision of a few kilovolts.

A cylindrical electrode just in front of the target generates a timing signal when the ion bunch passes through it. Neutrons produced in the target travel a distance L, typically 1 to 10 m, to the detector, where their arrival produces another electronic signal. We measure electronically the time interval between a neutron's birth and its detection. Given the flight path L, an online computer can calculate the velocity and therefore the energy of the neutron.

With this apparatus, we can measure a profile in a few minutes to an hour, depending on the concentration. The beam energy and the neutron reaction cross section determine the maximum depth that can be profiled. With our present equipment this depth may be up to 50 μm.

Because the neutron loses no energy to the target, the remaining target material beyond the neutron-production site does not affect the measurement and the sample may be thousands of times thicker than the maximum profiling depth. This allows us to profile self-supporting targets, small samples on thick backings, or even a piece of production material. Also, the sample need not be small enough to fit into the vacuum chamber; we can bring the probing beam out of the machine through a thin window and bombard the target in air.

One of the advantages of this profiling technique is that, except for minor radiation damage, it is nondestructive. This means that we can determine the

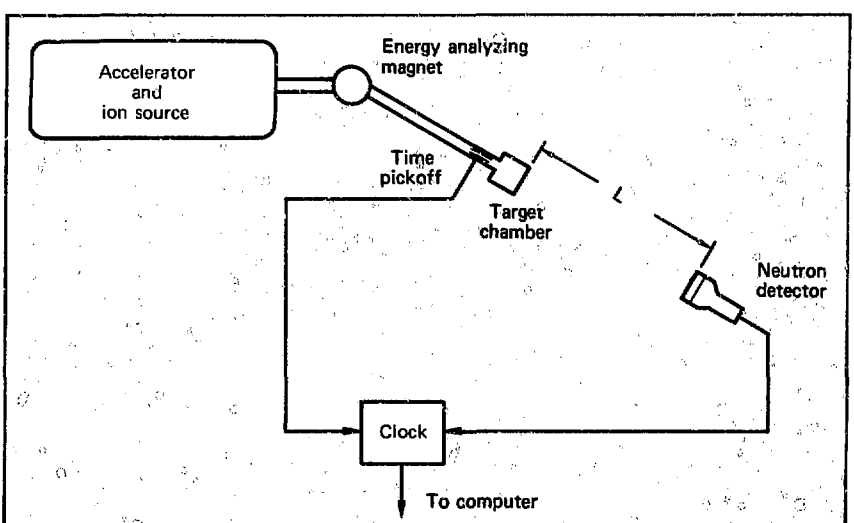

Fig. 3. Equipment for measuring the hydrogen-isotope depth profile in a target. The pulsed ion source provides bunches of hydrogen ions that the accelerator forms into a high energy beam. The analyzing magnet directs only those ions of a particular energy into the target chamber, where they bombard the target. Some of the neutrons fall on the neutron detector after traveling a distance L. For each neutron detected, the clock records how long it took to cover this distance. From the timing data, an online computer produces neutron energy spectra and profiles of hydrogen-isotope concentration.

hydrogen profile without sacrificing the specimen. It also means that we can follow a process, step by step, with consecutive profiles on the same specimen. We can, for example, observe hydrogen-profile changes as a function of temperature.

Another advantage is that the test involves hardly any sample handling. This greatly simplifies the problem of measuring hydrogen profiles in toxic, explosive, or radioactive materials.

In addition to flexibility, versatility, and convenience, concentration sensitivity and depth resolution are important factors in judging the utility of this technique. Sensitivity is determined by neutron and gamma-ray backgrounds and by the radiation dose the sample can take without changing the distribution to be studied. To date we have achieved a sensitivity of one part per million for tritium in copper.

Depth resolution depends on various factors. Near the front surface of the material, it is limited by the overall energy resolution of the apparatus. As we go deeper into the target, energy straggling of the probing ion beam in the target material becomes the dominant factor. Figure 4 shows how the various factors combine to determine the overall depth resolution for deuterium in titanium. Over the first 10 μm, the depth resolution is uniform at about 0.6 μm.

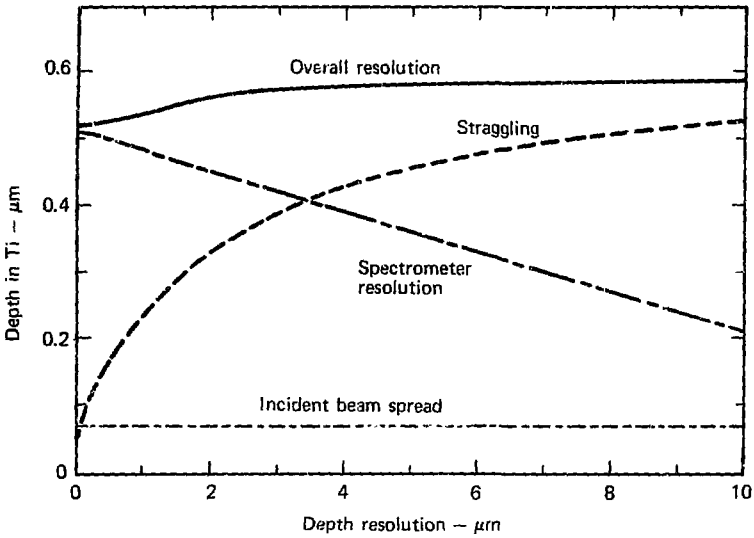

Fig. 4. Factors affecting depth resolution and how they change with depth for deuterium in titanium. The incident deuteron energy is 1.5 MeV, the neutron flight path is 10 m, and the spectrometer time resolution is 1.5 ns. Similar curves, differing in detail, apply to other combinations of bombarding ion and target material. The incident beam spread makes a constant contribution regardless of depth. The spectrometer resolution becomes less and less important with depth. Beyond 10 μm, straggling, which continues to increase gradually, is the dominant factor influencing resolution. The overall resolution in this case broadens from 0.6 μm at 10 μm to 1.5 μm at 50 μm.

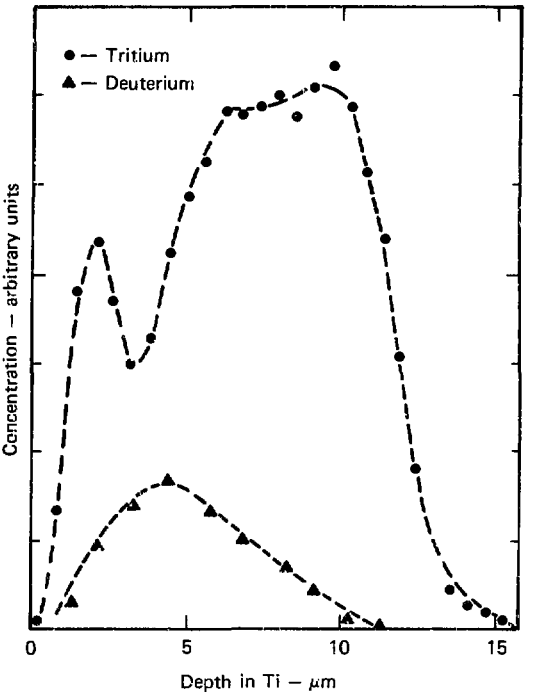

Fig. 5. Tritium and deuterium profiles in a titanium target after bombardment in the RTNS accelerator with 31 C/cm² of deuterium ions. Some of the deuterium has become implanted in the target, and some of the tritium, whose profile originally was similar to that in Fig. 2, has been replaced. Most of the original tritium is still present, however, and only a small fraction of the incident deuterium stayed embedded.

Even at 50 μm, depth resolution has worsened only to about 1.5 μm.

The depth resolution of our equipment is adequate for most purposes, and is at a practical optimum. None of the ways by which we might, in principle, improve resolution, such as shortening the ion-beam burst or increasing the neutron flight path, can have any effect on the ion beam's energy straggling. The improvement would therefore be marginal at best, and it would almost certainly be won at the cost of reduced concentration sensitivity.

The first application of this depth profiling technique was in our study of how bombardment with deuterons depletes the tritium bound to a titanium layer in the neutron generator target of LLL's Rotating Target Neutron Source (RTNS). Figure 5 shows depth profiles of tritium and deuterium remaining in the target after 31 C/cm² of bombardment. Only 15% of the initial tritium content of the target has been outgassed, while less than 10% of the injected deuterium remains. This suggests that some nonequilibrium process is at work. Evidently

deuterium is released 5 to 10 times as readily as tritium. A better understanding of this process could lead to improved target lifetime and performance.

Future developments with this technique involve an experiment with collaborators at the Los Alamos Scientific Laboratory to determine the feasibility of probing the hydrogen depth profile with a triton beam. We had a successful preliminary run, but the background was much higher than usual. We will have to improve the target chamber and the shielding before we can estimate what the ultimate sensitivity will be. Once we determine the sensitivity and limitations of this method, we plan to add a tritium source and a dedicated target chamber to the LLL Cyclograaff accelerator and to develop suitable computer software for providing a routine analytical service.

Key Words: deuterium — diffusion; deuterium nuclear reactions; hydriding; hydrogen embrittlement; hydrogen isotopes; rotating target neutron source; tritium nuclear reactions.

For Further Reading

An example of tritium profiling with a proton beam is described in J. Davis, J. Anderson, and H. Lefevre, "Depth Profiling of Tritium by Neutron Time-of-Flight," in *Radiation Effects and Tritium Technology for Fusion Reactors*, J. Watson and F. Wiffen, Eds. (Oak Ridge National Laboratory, Rept. CONF-750989, vol. IV, 1976), p. 187.

PHYSICAL SCIENCES

DISPLAY: An Interactive Picture Editor

DISPLAY is one of the latest in a series of utility programs for plotting numerical data and displaying it in graphical form. The graphic information is organized in a new way that makes it possible to manipulate individual picture elements, e.g., lines or points, providing a powerful editing capability. This same feature also enables the computer to operate on the entire image, interpolating as many frames as desired between two successive pictures and producing a moving picture of the transition from one to the other. The machine- and language-independent data structure of DISPLAY allows us to compare pictures generated by different machines, from different programs, written in different languages. The ability to alter and rezone data interactively has greatly reduced the turnaround time on our large hydrodynamic calculations.

Much of our computational work at LLL deals with predicting what will happen to structural parts subjected to violent stresses: explosions, high-speed impacts, shock waves, pulses of radiant energy, and the like. The hydrodynamic codes that do this are many and varied, but most approach the problem by dividing the region of interest into a mesh consisting of a large number of small zones, and computing how the applied forces will affect the material in each zone and how each zone will affect those around it.

One problem with this approach is that the final result, the shape and location of each zone at many intervals throughout the time period, adds up to an enormous quantity of data. Originally this output was in the form of printouts, page after page filled with columns of figures. The only way to see what had happened to the original structural part represented by these figures was by tedious hand plotting.

Another problem had to do with computer time. After each cycle, the program searches through all the zones for the one in which the "transit time" – the time it takes for a sonic signal to cross the zone – is the smallest. Then it sets the time interval for the next cycle to be less than this transit time. (It has to do this; a fundamental assumption of the whole calculation is that, within a given time interval, each zone can affect only those zones that touch it.)

When the zones are all reasonably sized, this causes no trouble. If a zone gets crushed down to almost

Contact Jeffery H. Rowe (Ext. 8621) for further information on this article.

nothing, however, or stretched very thin, both the transit time and the time interval per cycle approach zero. Each cycle takes up just as much computer time but makes less and less headway toward a solution; the computer keeps right on running but gets nowhere.

The only way to get the computer to finish the computation is to replace the compressed mesh with another that has only reasonably sized zones. This used to mean, first, stopping the computation, printing out the data, and hand plotting the compressed mesh. Next, we identified each zone in the compressed mesh with its counterpart in the original mesh. Then we drew up a new mesh within the same boundaries as the compressed mesh, and wrote a computer program outlining the point-to-point conversion from the compressed mesh to the new mesh. This was a slow and costly process.

A third problem with this approach was that all the human intervention led to large uncertainties in the final solutions. There was too much room for error, too much subjective judgment in the intermediate steps. Design calculations had to proceed in tiny steps, alternating with frequent, confirming hydrodiagnostic experiments. On some complicated designs, we might have 150 or more of these tests, spread over many months.

Early Solutions

The first big step in attacking these problems was to teach the computer to draw crude pictures of the problem mesh on a cathode ray tube (CRT). This eliminated hand plotting and showed us at once the strains and distortions taking place. We could also put a time limit on individual iterations, so that the program would display the last complete mesh before a zone got too small. Then we could, in theory at least, revise the mesh and proceed.

These early graphic displays had serious limitations, however. For one thing, the view they showed was determined in advance and might not include the part of the mesh that was in trouble. For another, the scale might be either too big or too small, causing us to miss significant details. The only way to get a revised view of the same calculation was to start over at the beginning, with new directions for scale and final location, and run the whole calculation again.

Some of these difficulties were overcome with a computer-driven plotter, which operated on the program output to draw graphs to any desired scale on paper. This eliminated rerunning a faulty program over and over just to locate and unscramble a mesh defect. The plotter was slow, however; it was still a time-consuming chore to find the fault and rezone the mesh.

The next big step was the introduction of time sharing and the television monitor display system (TMDS). They restored the CRT as the major means of viewing a problem mesh. Figure 1 represents a TMDS display of a defective mesh. Time sharing also made it possible to process the display online, manipulating the point of view, the scale, and even producing cross sections of three-dimensional models. We could make several pictures of a scrambled mesh at different magnifications, for example, and view them simply by changing frames on the TMDS.

But for all its flexibility and power, the time-sharing interactive TMDS had one major drawback. It could only graph the program output as generated by the computer, warts and all. It was still up to us to spot these flaws, to analyze the results and figure out where things went wrong, and finally to devise the appropriate correction, often by trial and error. With everyone vying for time on the computer, this too could be a time-consuming process.

An associated difficulty had to do with communication from one program to another, or from one machine to another. Some complex problems are best handled by x parts, with different programs computing the various parts separately. Special programs handle the physics aspects of the boundary region between the parts, assuring that the solutions are at least not contradictory.

Picturing the two solutions is a problem, however. The crunch comes at the interface, getting the two incompatible meshes to link up. This difficulty is compounded when we try to join solutions coming from two different machines, solutions that may not even be in the same format.

Interactive Plotting

Most of these difficulties are resolved with the interactive plotting routines that we have been

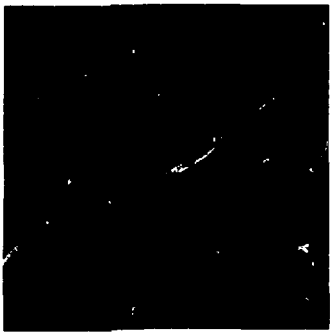

Fig. 1. A defective mesh formed on a 35-mm film plotter by the DISPLAY code. Color contrasts indicate two different materials. Radial lines are also colored differently from the circular arcs for ease in distinguishing them in the region of the defect (above). The first step in repairing the mesh defect is to enlarge the image of the region (upper right). Separate commands (with the aid of a cursor, if necessary) then move individual lines back into place to produce a regular mesh. A slight flattening of the circular arcs indicates the repaired area (right).

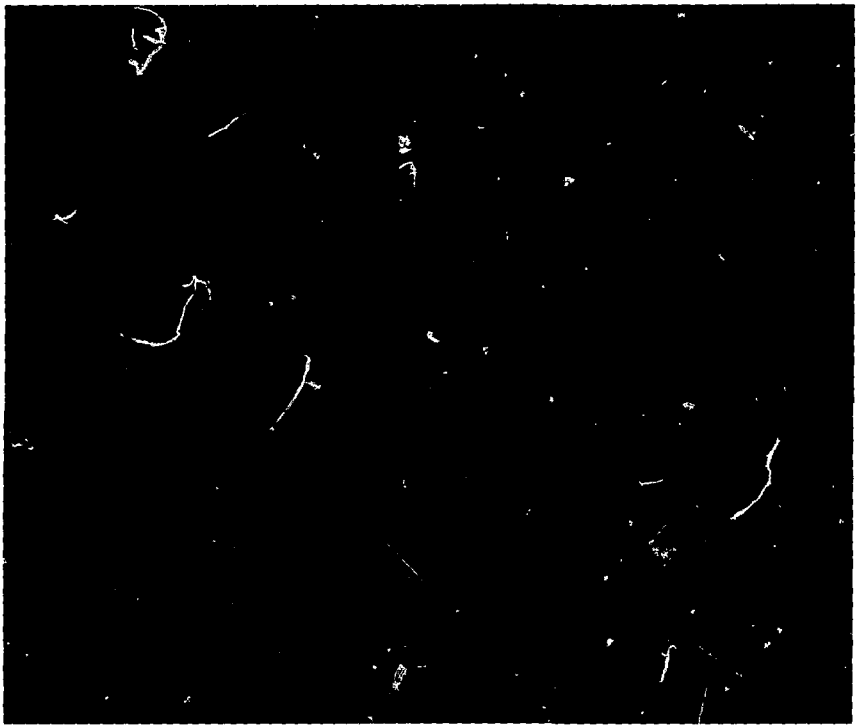

Fig. 2. A three-dimensional surface plotted from a single picture element containing three descriptors plus control data. Other picture elements might be small areas of a mesh, abstract symbols, text, lines, or even single points.

developing and refining over the last few years; DISPLAY and DPPAC form a good example. DPPAC is the subroutine library package that serves as a method of linking to DISPLAY. This library translates the program output into a "data base": a file that tags points, lines, planes, and three-dimensional surface plots in a picture, each with its own "descriptor." DPPAC allows us to manipulate, through DISPLAY, *not just the image as a whole but individual picture* elements. Figure 2 is a three-dimensional surface that was plotted from a single picture element containing three descriptors.

Having the parts of a picture defined as elements means that we no longer need to bother with identifying which zone in the original mesh has been compressed to nothing. Now we can operate on the scrambled mesh directly, untangling it bit by bit while the computer faithfully records every move and translates it into the appropriate changes to produce the desired final mesh. A convenient cursor that we can move about on the CRT display enables us to point out the items to be changed, one by one, as we enter our commands. Figure 1 suggests how this process operates.

At the same time, this way of organizing graphic information lets us superimpose different parameter runs of the same problem for direct comparison, or combine pictures produced by different programs or even by different machines. In the latter case, we simply display them side by side, adjust the images to a common scale if necessary, and smooth out the interface boundary. DISPLAY keeps track of all the required changes and tells the various source programs, each in its own terms, what to alter to bring about the desired combined image.

Another handy application is in making movies. Suppose a calculation gives us a series of views of some process, separated in time but all from the same viewpoint. DISPLAY will generate any desired number of intermediate frames between any two views, in effect supplying the animation from a story board presentation. The picture may be in black and white or, with the addition of a few simple commands, in a rainbow of colors. Figure 3 shows a film strip animated in this way.

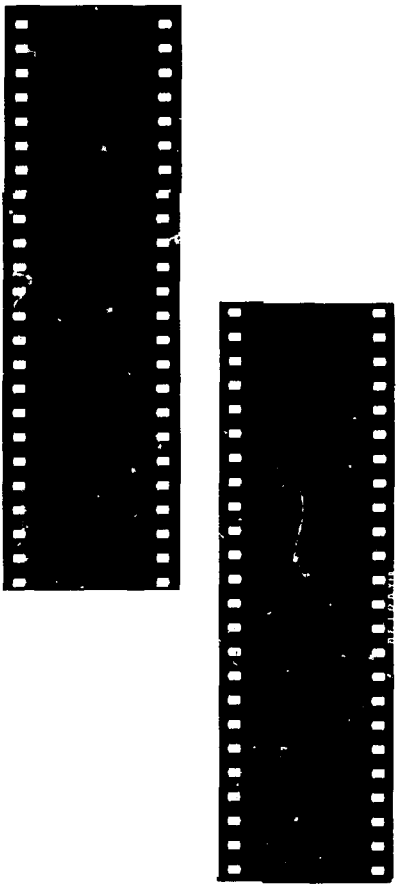

Fig. 3. A film strip produced by key-frame animation with DISPLAY. This sequence, starting from the top, shows how four separate disturbances grow and coalesce into a single disturbance. The first and last frames make up the original input; DISPLAY interpolated the frames in between. This sequence would play out in less than a second, but DISPLAY could have stretched it to any desired length by interpolating more frames.

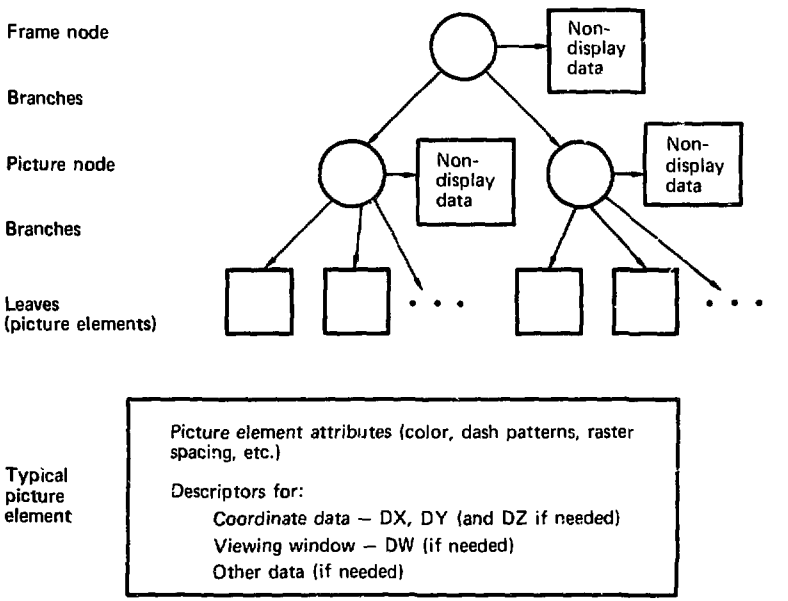

Fig. 4. Tree-structure diagram for a frame in a DISPLAY data base. Nondisplay data includes such items as computed data limits, grid sizes, contour levels, and so forth. The nondisplay data at each node supersedes similar data at all lower nodes. The branching tree structure of this data base makes it possible to edit individual elements without affecting the rest of the picture. Each picture element, for example, contains only the information needed for drawing a particular part of the picture. Each descriptor in the picture element consists of two parts, a length portion telling how many points the element contains (DISPLAY will fill in a line connecting the points indicated) and an address portion telling where to find the coordinates. (The coordinates occupy contiguous memory locations.)

The feature that makes DISPLAY and the other interactive plotting routines so useful is the way their graphic information is organized. Previous plotting routines operated directly on the output data, either plotting it immediately or converting it into a file tailored to a particular plotting device: a microfilm plotter, the TMDS, or a remote hardcopy printer, for example. Once in this form, the data could no longer be plotted on any of the other plotters, the original output ceased to exist.

DISPLAY saves the original data, preserving the option of plotting on different graphic devices. DPPAC rearranges the original output into a DISPLAY data base compatible with any of them, and stores it in accessible form so that it may be edited. Figure 4 outlines the organization of the DISPLAY data base.

These two features of the DISPLAY data base, compatibility and accessibility, open up an enormous range of possibilities. We can dissect pictures, deleting unwanted features. We can manipulate the scale, making enlargements of significant details. We can create entirely new pictures, pieced together from portions of others.

A picture element in this system may represent anything: a point, a line, an area, even a line of text or an electronic symbol. Each element is present in the data base as three entities: a plot mode number, control data, and coordinate data. The plot mode number indicates such things as the frame control, the scaling and mapping control, and whether the data is one, two, or three dimensional, or text. The control data sets forth how the element is to be drawn, whether it is to be colored or dashed, whether an area is to be shaded, and so forth. The coordinate data tells how big the element is and where it goes in the picture.

All the coordinate data – and much of the control data – of a picture element is in the form of descriptors. These are computer words that contain, not the data itself, but directions for finding it. Every descriptor has two parts, a length portion that tells the computer how many contiguous data points it will have to look up for this element, and an address portion that tells it where to look. The coordinate data, for example, may still be back in the source program.

When DISPLAY plots, it draws the picture, element by element. It looks up the x and y coordinates specified in a set of descriptors and, like a child playing connect-the-dots, fills in a line between the points according to the directions in the control data. For a straight line, only the end points need to be specified. For a curve we must supply intermediate points.

DISPLAY is an evolving system. Its machine- and library-independence makes it function equally well on the CDC 7600 and STAR computers; this independence also means that DISPLAY will be easy to adapt to any future computers we may acquire. Many more capabilities can be imagined for it than have so far been implemented. At present, for example, the system is limited to rectangular plotting because that is in demand. If a need for polar coordinate graphing comes up, that will be easy to add.

At present we are working to improve the three-dimensional plotting mode and the data structure for object and surface plots. We plan to develop a truly machine-independent data representation for coordinate data. We are also looking forward to providing the ability to copy picture elements from one data base to another.

DISPLAY is a solution to the problem of establishing a common data-base and picture-editing system for scientific graphical information. The ability to alter and rezone data on line has greatly improved the turnaround time for many LLL hydrodynamic computations. Making it easy to generate movies with key-frame interpolation has been a big help in the presentation of these and other LLL projects.

Key Words: computer graphics; DISPLAY; hydrodynamics – computations; television monitor display system; TMDS.

For Further Reading

J. Rowe, *DISPLAY*, Lawrence Livermore Laboratory, Rept. UCID-30081 (1973).

J. Rowe, *TVGRAPHICS*, Lawrence Livermore Laboratory, Rept. UCID-30020 (1971).

PAST TITLES

Articles in the *Energy and Technology Review* have been organized into subject areas approximately corresponding to the Assistant Administrators' areas of responsibility in the Energy Research and Development Administration. These subject areas are listed below with references to some recent articles in each category. (A semiannual index appears in the June and December issues.)

Conservation

The Methanol Engine: A Transportation Strategy for the Post-Petroleum Era (*December 1976*)
Flywheel-Battery Hybrid: A New Concept for Vehicle Propulsion (*June 1976*)

Environment and Safety

Phantom Construction: Building a Torso Manikin for Whole-Body Counting (*December 1976*)
Getting the Facts About Ozone (*November 1976*)
Characterizing Stack Emissions from Coal-Fired Power Plants (*October 1976*)
LLL Biomedical and Environmental Research Program Overview (*May 1976*)

Fossil Energy

Underground Coal Gasification in the U.S.S.R. (*September 1976*)
Forecasting the World's Crude Oil Supply (*July 1976*)
Modeling the Pyrolysis Phase in *In Situ* Coal Gasification (*April 1976*)

National Security

Imaging Implosion Dynamics: The X-Ray Pinhole/Streak Camera (*December 1976*)
Soviet Experience with Peaceful Uses of Nuclear Explosions (*September 1976*)
Electric Gun: A Versatile Tool for Studying Explosive Initiation (*August 1976*)
The Slapper: A New Kind of Detonator (*July 1976*)
LLL Laser Program Overview (*February 1976*)

Nuclear Energy

Safety and Safeguards: Defining the Issues (*October 1976*)
Automated Uranium Assays (*July 1976*)
Laser Excitation Spectroscopy of Uranium (*February 1976*)

Physical Sciences and Engineering

Recognizing the Pattern of Crime (*November 1976*)
Taking the Moon's Internal Temperature (*November 1976*)
Neutron and Gamma-Ray Transport Experiments in Liquid Air (*July 1976*)

Solar, Geothermal, and Advanced Energy Systems

National MFE Computer Center: 1976 Update (*December 1976*)
LLL Magnetic Fusion Energy Program: An Overview (*June 1976*)
Control of Geothermal Scaling and Corrosion (*March 1976*)

GPO 789-038/10

Printed in the United States of America
Available from
National Technical Information Service
U.S. Department of Commerce
5... Port Royal Road
Springfield, Virginia 22161
Price: Printed Copy $4.00; Microfiche $2.25